ELSEVIER

S0032-3861(96)00241-8

Polymer Vol. 37 No. 18, pp. 4155–4165, 1996

0032-3861/96/$15.00+0.00

Structural effects on free volume distribution in glassy polysulfones: molecular modelling of gas permeability

Satu Niemelä, Jukka Leppänen and Franciska Sundholm*
Laboratory of Polymer Chemistry, University of Helsinki, PB 55, FIN-00014 HY Helsinki, Finland
(Received 20 October 1995; revised 23 January 1996)

Molecular mechanics and molecular dynamics have been used to build amorphous cells of 13 different aromatic polysulfones. The amorphous-state disorder was analysed in terms of pair correlation functions. Relaxed and equilibrated cells were generated and the cohesive energy density and the solubility parameters were calculated. Variations in the solubility parameters were related to polymer structure, and to experimental glass transition temperature, T_g, values for the polymers. The distribution of occupied and unoccupied space was evaluated by the technique of Voronoi tessellation of space. The distributions of the Voronoi polyhedra volumes are very broad, and have a bimodal or a trimodal character, which is related to the structure of the polymer. Experimental values for the permeability of helium and carbon dioxide molecules were related to the fraction of Voronoi polyhedra with volumes > 10.5 Å^3. The validity of the simulated polymer structures were further verified by comparison between the calculated values for the intersegmental spacings, and values measured by using X-ray diffraction. Copyright © 1996 Elsevier Science Ltd.

(Keywords: polysulfones; molecular modelling; gas permeability)

INTRODUCTION

Polysulfones are high-performance thermoplastics that find many commercial applications. High barrier properties are of interest because of the potential use of the polymers in packaging and protective coatings[1]. Despite the increase in technological demand, the molecular features responsible for gas separation, gas permeability, solubility and diffusion in such systems are still not well understood. The reality of present technology is that a single polymer layer with sufficiently low permeability to gases and water, and with other characteristic properties necessary for end-use applications, is not yet available. Our aim in this molecular modelling study is to establish the possible chemical compositions and the structural factors that influence such permeability.

Gas transport in polymers is a complex process which is controlled by the total free volume, the distribution of the free volume, the dynamics of the free volume, and by the solubility of the gas molecules in the polymer. The gas molecules undergo transport in a polymer in the glassy state from cavity to cavity, aided by minor segemental motions. The permeability and the diffusivity of the gas is dependent on the concentration of the cavities which can receive the gas molecule. Thus, gas transport is determined by the distribution of free volume in the system. Development of molecular modelling has made it possible to simulate polymer microstructures, and to calculate the free volume distribution in polymers.

We have chosen various polysulfones as candidates for our study, with the gas permeability data of these polymers being available in the current literature. The structures of the polymers used in this present work, and their corresponding abbreviations, are presented in *Figure 1*. The properties of the polymers are collected together in *Table 1*. Bisphenol A polysulfone has been used extensively as a material for membrane-based gas separation[2,3] and its gas transport properties have been studied in great detail[4–7]. Ghosal *et al.*[8] report the determination of gas permeabilities of Radel A-100 polysulfone, and have compared these with data obtained for the bisphenol A polysulfone[5,6] and poly(ether sulfone)[9]. Thus, gas permeability and selectivity are believed to be dependent on the polymer packing properties, and the interactions between penetrant and polymer[10]. These properties have been influenced by modifications in the chemical structure of the polysulfones. The effect of structural symmetry of the phenylene linkages, and the methyl group placement, on the properties of polysulfones have been investigated[11]. It was shown that polysulfones with unsymmetrical structures have lower gas permeabilities and higher selectivity coefficients than their symmetric counterparts. Polysulfones containing *meta*-phenylene linkages were found to have lower glass transition temperatures and lower fractional free volumes than polysulfones with *para*-phenylene linkages[10]. Dimethyl substitution in the bisphenol aromatic rings increases both the glass transition temperatures and the fractional free volumes. The chains of the unsymmetric polymers appeared to be more efficiently packed, and had greater

* To whom correspondence should be addressed

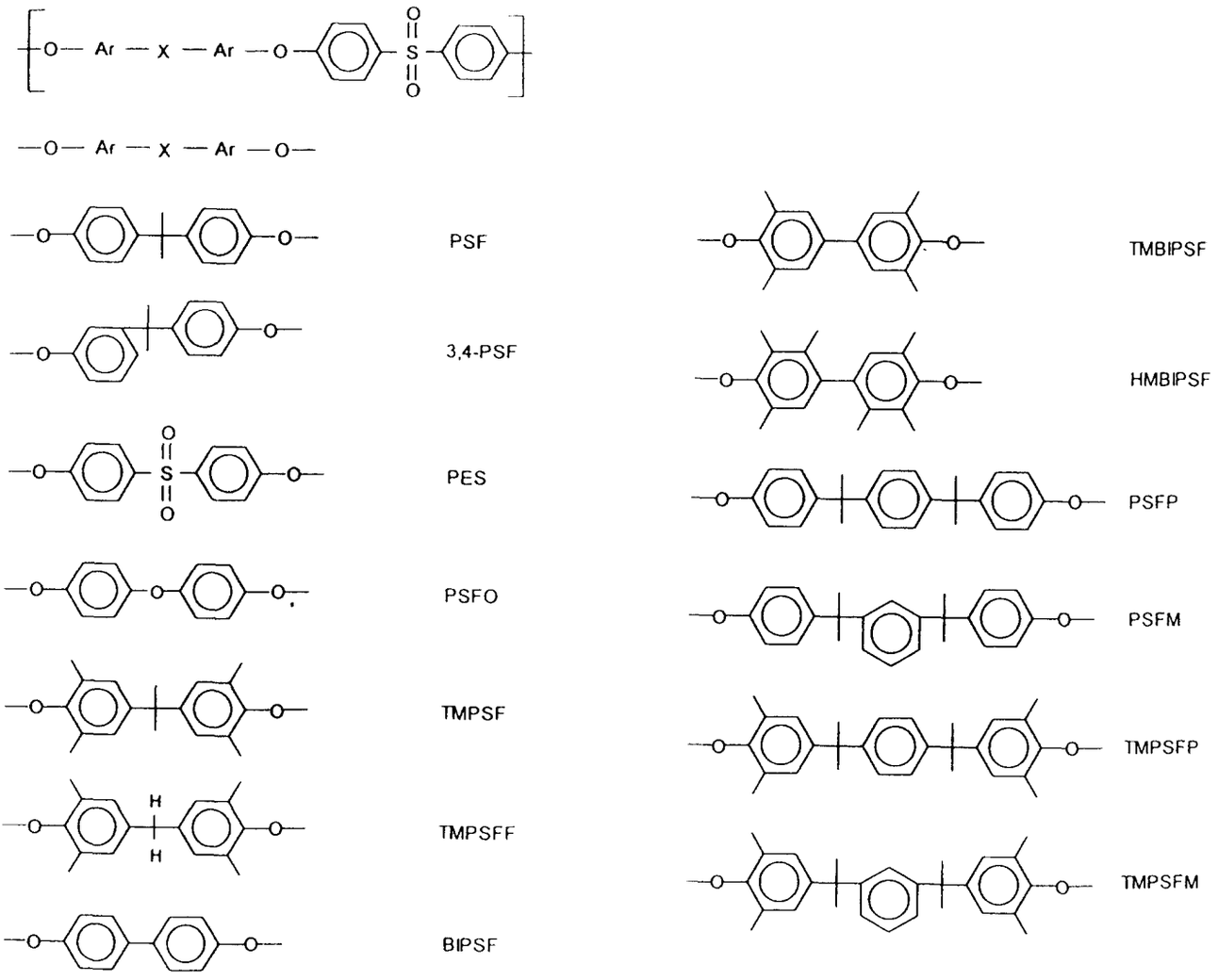

Figure 1 Structures of the polymers used in this study, and their abbreviations

Table 1 Properties of the polysulfones examined in this study

Polymer	T_g[a] (°C)	Density (g cm^{-3})	Fractional free volume	V^{f}[b]	Experimental d-spacing[c] (Å)	Calculated d-spacing[c] (Å)	Solubility parameter ((J cm^{-3})$^{0.5}$)	P_{CO_2}[d]	P_{He}[d]
PSF	186	1.24	0.156	0.4861	4.9	5.2	20.0 ± 0.48	5.6	13
PSF34	156	1.249	0.149	0.4831	4.9	5.3	18.73 ± 0.87	1.5[e]	9.3[e]
PES	225	1.370	0.151	0.4805		5.1	20.76 ± 0.70	2.8	10
PSFO	181	1.33	0.150	0.4773	4.8	5.0	19.96 ± 0.96	4.3	8
TMPSF	230	1.151	0.171	0.5099	5.3	5.8	18.71 ± 0.39	21	41
TMPSFF	232	1.184	0.163	0.5029	5.2	5.6	18.81 ± 0.52	15	29
BIPSF	231	1.291	0.154	0.4678	4.8	5.0	21.42 ± 0.59	5.6	12
TMBIPSF	288	1.195	0.164	0.5038	5.3	5.7	19.71 ± 0.43	31.8	36
HMBIPSF	295	1.144	0.178	0.5123	5.3	5.9	18.17 ± 0.22	25.5	53
PSFP	191	1.191	0.156	0.4804	4.9	5.4	20.13 ± 0.58	6.8	14
PSFM	140	1.201	0.151	0.4820	4.7	5.3	19.59 ± 0.63	2.8[e]	11.7[e]
TMPSFP	214	1.127	0.168	0.5009	5.2	5.6	18.25 ± 0.48	13.2	32.0
TMPSFM	175	1.141	0.158	0.4966	5.1	5.7	17.22 ± 0.53	7.0	21

[a] Values from refs 7, 10 and 11
[b] Fraction of Voronoi polyhedra > 10.5 Å^3
[c] Values from refs 10 and 11
[d] Measured in units of 10^{-10} (cm^3 (stp) cm s^{-1} cm^{-2} cmHg^{-1}); values, measured at 10 atm (1.101 MPa), taken from refs 10 and 11
[e] Measured at 1 atm (0.11 MPa)

mobility constraints than their symmetric counterparts, which thus influence their permeation behaviour.

Another structural feature which affects the permeability is that of chain flexibility. In the glassy state, where the segmental mobility is low or even absent, the permeability of the polymer is governed by the free volume[12–14]. The larger the free volume, then the higher will be the permeability. A rigid polymer chain and bulky substituents normally result in glassy polymers, but can also lead to a low packing density, large interchain distances, and large free volumes. A flexible polymer backbone allows the polymer chains to relax to a small free volume before they are frozen at the glass transition T_g, but the T_g, however, is usually low.

Attempts have been made to correlate the gas permeability in polymers with various measures of the free volume. McHattie *et al.*[15] calculated the free volumes of a number of polycarbonates on the basis of mass and volume by using the Bondi group contribution methods[16], and the method of Sugden[17]. McHattie *et al.*[6,7,18] also studied a series of tetramethyl-substituted polysulfones with respect to their gas transport properties, and related these to calculated values of the free volume. They found, in both cases[15,18], good agreement between the gas permeability values and the values of fractional free volume.

The treatment of volumetric changes, i.e. changes in free volume distribution, in glassy polymers has proven to be complicated due to the non-equilibrium state of these materials. Jordan and Koros[19] have described a model which unites concepts from the lattice-fluid equation of state, and the hole-filling model. An important feature of this model is its ability to relate an independent description of the glassy state to gas sorption and dilation. The characterization involves a measure of the hole size distribution, with the polymers under study being polycarbonates. Tamai *et al.*[20] report the molecular simulation of permeation of small penetrants through membranes. The free volume was analysed in terms of free volume clusters by using a water molecule as a probe. It was shown that the channels through which the small molecules permeate are comparatively narrow. Chow[21] has derived a statistical mechanical theory of the density fluctuations of holes in amorphous polymers. The hole volume distribution is related to two structural parameters, namely the energy of hole formation, and the lattice volume. The calculated results are consistent with measured values for an epoxy polymer resin.

Free volume (hole) distributions have also been studied by molecular dynamics. Rigby and Roe[22] treated dense systems of alkane chains which were subject to potentials restricting the molecular geometry and interactions with neighbouring chains. The distribution of free volume in the systems was evaluated by the technique of the *Voronoi tesselation of space*, and by the enumeration of cavities when hard spheres were assumed to be placed on atomic centres. The distribution of volumes often exhibits a bimodal or a trimodal character, and the cavities change shape and size with time. The results indicate a spatial inhomogeneity in the density. Although this method requires further refinement for the correlation of the structure and properties of polymers with gas sorption and dilation in glassy polymers, we have found it useful in predicting synthetic routes to permselective polymers.

In this present paper we report the results of molecular modelling of a number of amorphous polysulfones, in which the aim is to relate the chemical structure, the intra- and the intermolecular distances, the free volume and the distribution of sizes of the holes comprising the free volume, defined by using the technique of Voronoi tessellation of space, with the gas permeability of the membrane. We have chosen helium and carbon dioxide gas for the permeability correlations, since experimental data for these gases can be found in the literature. The modelling will be further developed in order to deal with other molecules diffusing into the polymer matrix.

THE SIMULATION METHOD

The representative microstructures of 13 different aromatic polysulfones have been constructed. The construction is based on a knowledge of the intra- and intermolecular forces between atoms, which is described by a force field. The force field acts as an intermediary in the transformation from the microscopic level to the macroscopic bulk properties. The models built are amorphous, non-oriented, non-crosslinked polymers. The constructed polymers are subjected to relaxation processes in order to reach an equilibrium state. Similar schemes have been applied to polymer systems such as polypropylene[23,24], polycarbonates[25,26], polysulfone[27,28], poly(*cis*-1,4-butadiene)[29], and polystyrenes[30,31].

The atom-based models of the amorphous polysulfones are constructed by packing polymer chains into a cube by using periodic boundary conditions[32]. The amount of monomers in the chain was chosen so that the cell size was close to 20 Å in length. Using this criterion, the number of monomer units in each cell varies between 8 and 12. Since the polysulfone chain is very rigid, and the monomer unit is very large, packing to give the experimental density is difficult to achieve. Problems arise from overlapping of the polymer chains, and catenation of the rings in the chains. The initial density in the constructed cell was 0.8 g cm^{-3}, which is considerably less than the experimental value. The structure refinement was carried out by using, alternatively, molecular mechanics minimization and molecular dynamics. The initial high-energy structures were relaxed by using steepest descent minimization until the average deviation of the energy derivatives was less than 5 kcal mol^{-1}. The structures were then equilibrated using molecular dynamics at 298 K over a period of 5 ps. The final stage of the structure refinement runs involved conjugate minimization using convergence criteria until the energy derivatives were less than 0.1 kcal mol^{-1}. The cells were then compressed to the experimental densities (given in *Table 1*) by using molecular dynamics.

In order to relax the cell structures after compressing to the experimental density, molecular dynamics was performed at 800 K for 4 ps. The total potential energy was then minimized by using a conjugate gradient method until the root mean square (rms) energy derivatives were less than 0.01 kcal mol^{-1}. In the calculations of non-bonded interactions the cut-off distance was 8.5 Å. During compression, the shape of the cell was kept cubic, and during the molecular dynamics and

energy minimization procedures the density, and the structure of the cell, were kept fixed. Among the possible minimized cell structures, 8–10 of these were chosen, all of which had deviations in total energies which were well within 10%. The total energies were compilated from the partial energies of the force field that was used[33].

The validity of the relaxed cell structures was checked by calculating the pair distribution function $g_{\alpha\beta}(r)$[34,35]. A pair distribution function is defined as the probability of finding any two atoms α and β at a distance of r apart in the simulated structure relative to the probability expected for a completely random distribution at the same density.

The cohesive energy densities and the solubility parameters were calculated. In atomistic simulations for polymeric materials, the cohesive energy E_{coh} is defined as the increase in energy per mol when all intermolecular forces are removed, and the cohesive energy density is given by the following:

$$U_{coh} = E_{coh}/V \quad (1)$$

where V is the molar volume of the polymer. Details of this calculation have been described[23,36]. The cohesive energy density is related to an experimentally measurable quantity, namely the Hildebrand solubility parameter. The solubility parameter is defined as the square root of the cohesive energy density, as follows:

$$\delta = U_{coh}^{0.5} \quad (2)$$

The free volume distribution has been estimated by using the Voronoi tessellation method[34,35,37–39]. In this method, the vectors connecting all pairs of atoms in the system are perpendicularly bisected, and a large number of intersecting planes are generated. The polyhedron associated with a given centre is obtained by selecting the smallest of the polyhedra that are thus formed around it. The amorphous-state structure can be evaluated by a number of distributions, namely those of the polyhedron volumes, the total polyhedron surface areas, and the parameters referring to the ratios of the polyhedron surface areas and volumes. These statistical distributions were calculated for the polysulfones, respectively, as the average from all of the cell structures constructed. As a Voronoi polyhedron around an atom identifies its own available space, this can then be related to the void volume in a dense, amorphous polymer.

The packing of the chains, and the interchain distances in the polymer cells, were estimated by simulating the X-ray scattering patterns from the simulated structures. The scattering intensity of the amorphous structure is calculated by using the following relationship:

$$I(\boldsymbol{Q}) = 4\pi V \sum_{\alpha\beta=1}^{\nu} \sum \rho_\alpha \rho_\beta \int_0^\infty r^2 g_{\alpha\beta}(r) \frac{\sin(\boldsymbol{Q}r)}{\boldsymbol{Q}r} \mathrm{d}r \quad (3)$$

where V is the volume of the polymer amorphous cell, α and β are the different atomic species in the system, ρ_α and ρ_β are the atom densities, $g_{\alpha\beta}(r)$ is the pair distribution function for atoms α and β, and ν is the number of atom types. $\boldsymbol{Q} = (4\pi \sin\Theta)/\lambda$ is the scattering vector.

The molecular mechanics and molecular dynamics calculations performed in this work were carried out by using the DISCOVER software package, which includes the POLYMER module (Biosym Technologies Inc.)[39]. The PCFF force field[37] was used. The molecular mechanics and molecular dynamics calculations, and amorphous cell constructions, as well as the graphics, were all performed by using Silicon Graphics Personal iris 4D/30 and Indigo 2 workstations.

RESULTS AND DISCUSSION

The final relaxed amorphous cells of the polysulfones were analysed in order to study the internal structure of the model. After construction of the amorphous cells of the polysulfones some tension or compression may remain in the polymer structure. In addition, with low barriers between the various regions in the distribution of rotational angles ($< 3\,\mathrm{kcal\,mol^{-1}}$) there can be a population of chain conformations containing torsional angles that are not necessarily at the minima. Conformational analyses of the polymers were carried out by calculating the distribution of the backbone dihedral angles for several linkages and comparing these with potential energy maps calculated for the corresponding monomers. The linkages analysed included the diphenyl sulfone, the diphenyl methyl, the diphenyl isopropyl, the diphenyl ether, and the *ortho,ortho*-dimethylphenyl phenyl ether linkage. Representative potential energy maps of the single chain backbone rotations, and the distribution of the backbone torsional angles in the polysulfones that were studied are shown in *Figures 2–6*.

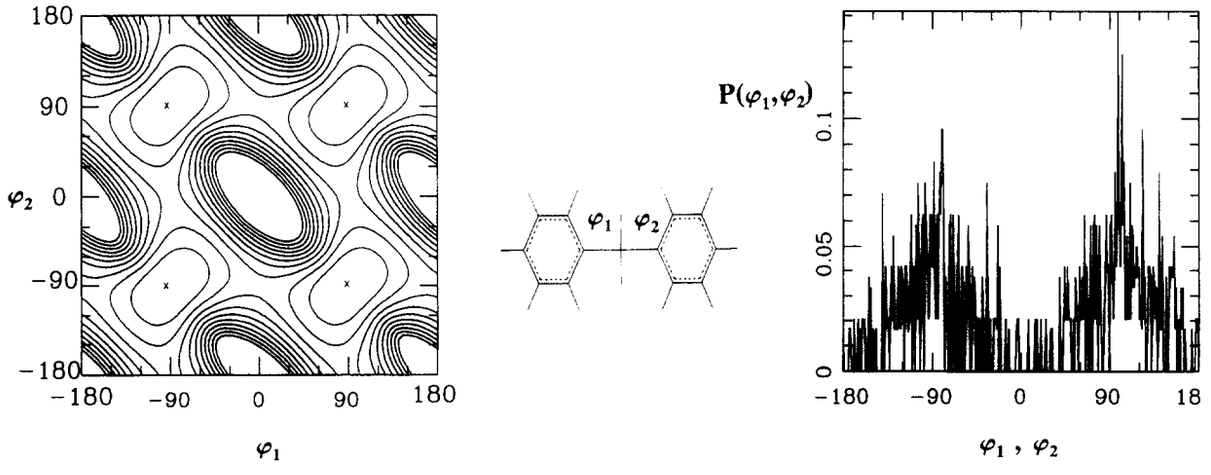

Figure 2 Calculated contour energy map and distributions of conformational states of S–C bonds of backbone rotations in diphenyl sulfone groups; increment is $1.0\,\mathrm{kcal\,mol^{-1}}$

The torsional angles are defined in the figures. The torsional angle calculations were carried out at 5° intervals. A dihedral angle of 36° between the aromatic rings in biphenyl moieties gives the minimum energy conformation with the force field that was used. The potential energy contour maps together with the corresponding distribution of conformational states shown in *Figures 2–6*, provide not only information on structure and chain conformation, but also information on the chain relaxation.

The S–C bond in the diphenyl sulfone linkage has a single minimum at $(\phi_1, \phi_2) = (\pm 90°, \pm 90°)$ (see *Figure 2*). Transitions between the minimal energy conformations can occur through narrow low-energy areas, with the barrier being ca. 2.8 kcal mol^{-1}. The results of this conformational analysis differ slightly from the results reported by Fan and Hsu[27], who report two minima, i.e. $(\pm 70°, \pm 70°)$ and $(\pm 110°, \pm 110°)$, for the C–S linkage, with an even lower energy barrier, 1.5 kcal mol^{-1}, between the minima. Fan and Hsu[27,28] used a force field in their calculations which was different from ours, which explains the difference in the results. We believe that our refined force field give more accurate results.

The energy contour map for the diphenyl methyl linking group is very similar to the map for the diphenyl sulfone group (see *Figure 3*). The minimum energy conformations occur with $(\phi_3, \phi_4) = (\pm 68°, \pm 68°)$ and $(\pm 112°, \pm 112°)$, with an energy barrier of ~1 kcal mol^{-1} between the minima. A number of chain conformations can therefore exist between the minima.

The C–C torsional angles in the diphenyl isopropyl unit are shown in *Figure 4*. The distribution of torsional angles is more localized than in the two previous cases, i.e. $(\phi_5, \phi_6) = (\pm 48°, \pm 48°)$ and $(\pm 138°, 138°)$, with the barriers to rotation being >3 and 1.6 kcal mol^{-1}, respectively. Hence the C–C bonds in the isopropyl group are more rigid than the unsubstituted C–C bonds, and also more rigid and localized than the S–C bonds. The conformational analysis of the diphenyl isopropyl group agrees reasonably well with previous results, although the rotational barrier reported earlier is higher than in this present work[27].

Analysis of the diphenyl ether C–O bond shows two minima of $(\phi_7, \phi_8) = (\pm 36°, \pm 36°)$ and $(\pm 146°, 146°)$ with energy barriers of >6 and 1.4 kcal mol^{-1}, respectively (see *Figure 5*). The diphenyl ether linkage in the polymer backbone is therefore very similar to the diphenyl propane linkage. In contrast, Fan and Hsu

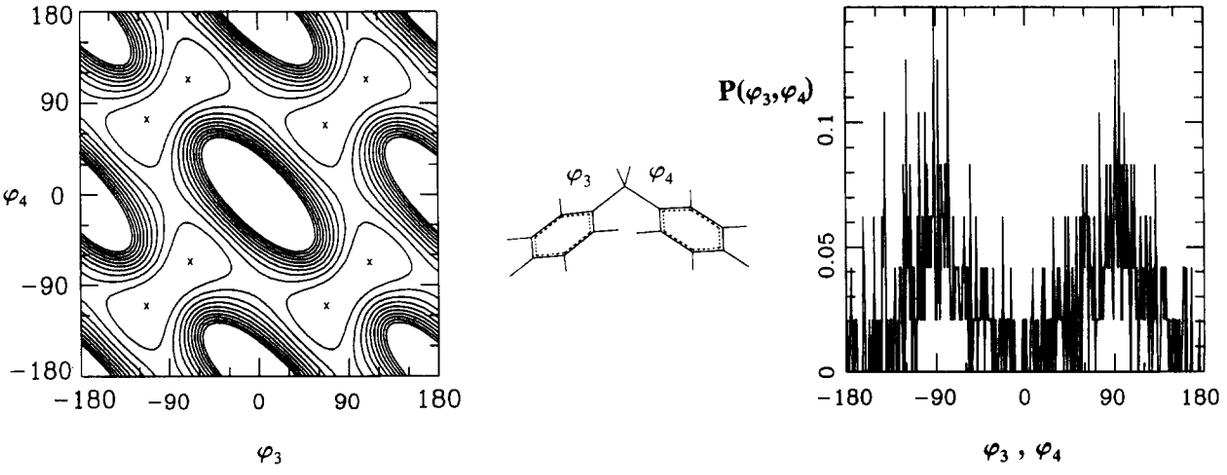

Figure 3 Calculated contour energy map and distribution of conformational states of C–C bonds of backbone rotations in diphenyl methylene groups; increment is 0.5 kcal mol^{-1}

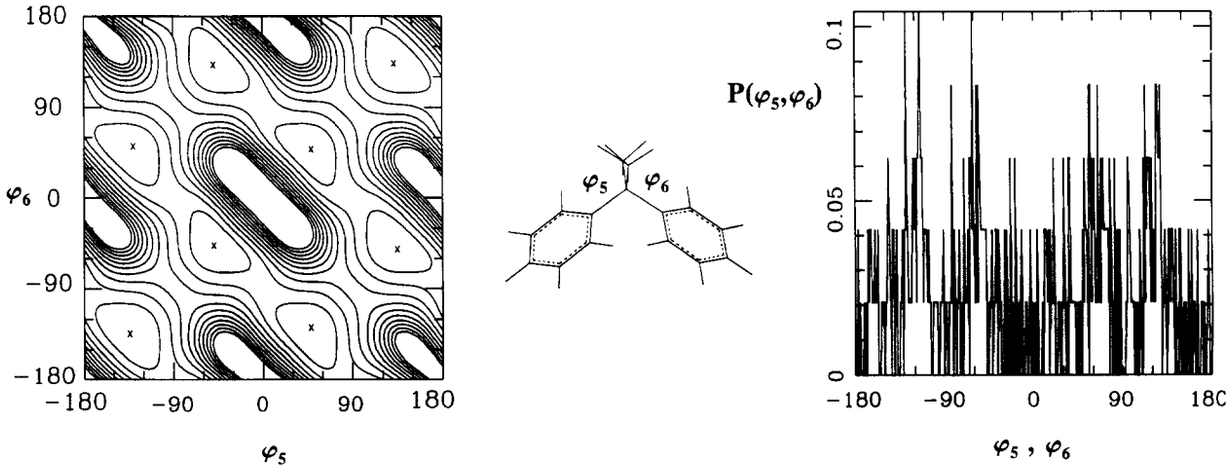

Figure 4 Calculated contour energy map and distribution of conformational states of C–C bonds of backbone rotations in diphenyl isopropyl groups; increment is 1 kcal mol^{-1}

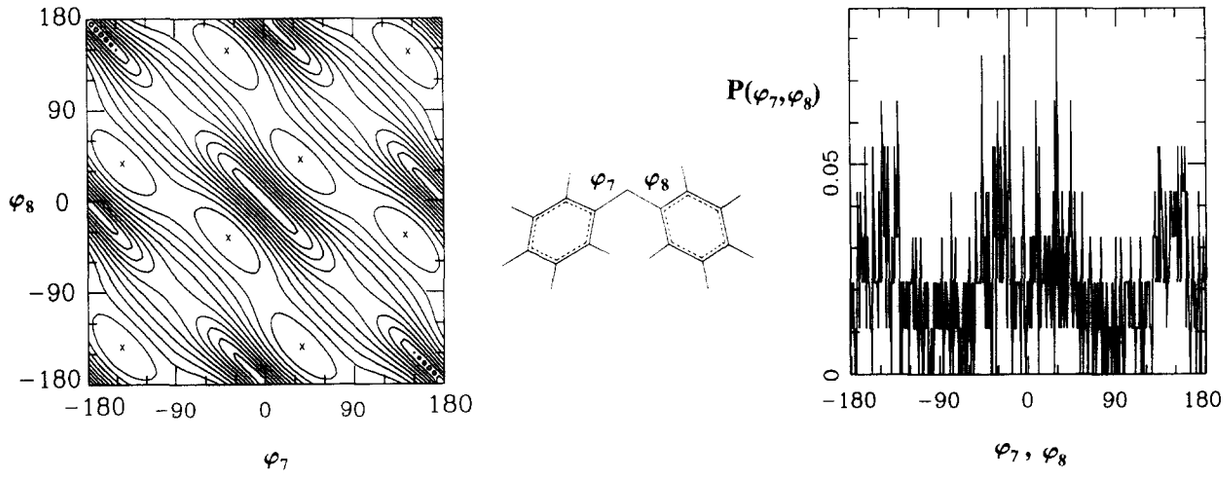

Figure 5 Calculated contour energy map and distribution of conformational states of C–O bonds of backbone rotations in diphenyl ether groups; increment is 1 kcal mol^{-1}

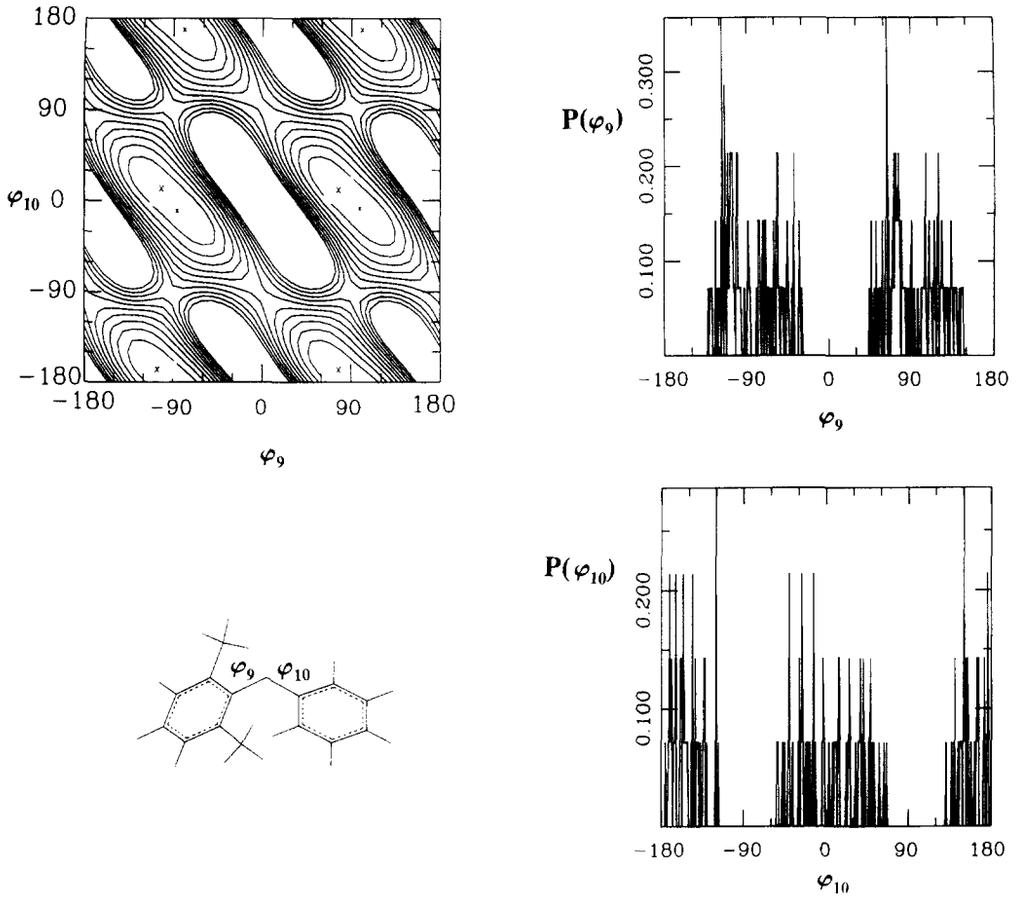

Figure 6 Calculated contour energy map and distribution of conformational states of C–O bonds of backbone rotations in *ortho,ortho*-dimethylphenyl phenyl ether groups; increment is 1 kcal mol^{-1}

report a conformation for the diphenyl ether group which is similar to the diphenyl sulfone group[27]. Again this difference is explained by the different force fields that were used.

An example of the influence of ring methyl substituents on the chain conformation is seen in *Figure 6*, where the energy contour map for the *ortho,ortho*-dimethylphenyl phenyl ether group is reported. The minimum energy conformation occurs with $(\phi_9, \phi_{10}) = (+75°, +12°)$, $(+75°, -169°)$, $(-75°, -12°)$, $(-75°, +169°)$, $(+105°, -12°)$, $(+105°, +169°)$, $(-105°, +12°)$ and $(-105°, -169°)$. The barriers to rotation are >5 and >7 kcal mol^{-1}, hence ring substitution has caused considerable stiffening of the chain, and ring flip relaxation of the chain is not possible.

The chain stiffening by methyl substituents in the aromatic rings is reflected in the values of T_g. The T_g of TMPSF is 54° higher than that of PSF, the T_g of TMBIPSF is 57° higher than that of BIPSF, the T_g of TMPSFP is 23° higher than that of PSFP, and the T_g

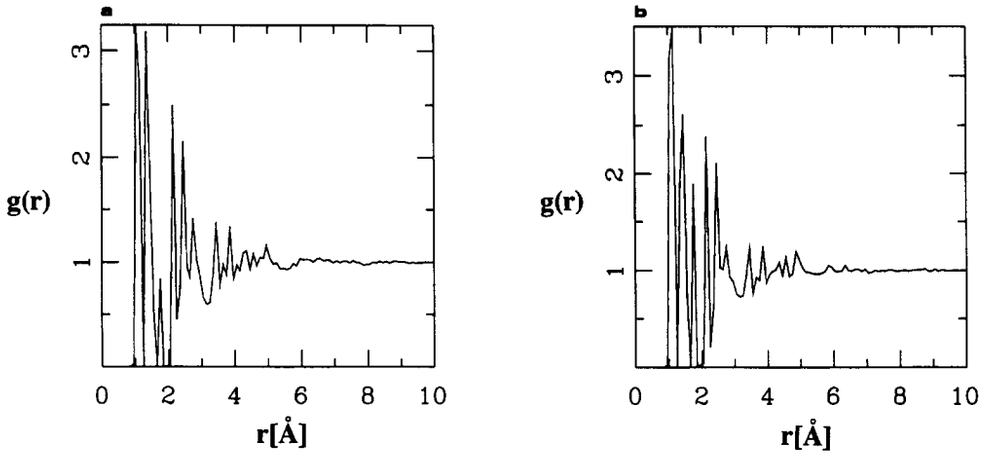

Figure 7 Total pair distribution functions for (a) PSF and (b) HMBIPSF

of TMPSFM is 35° higher than that of PSFM (see *Table 1*). The structure dependence of the T_g in polysulfones has also been discussed by Aitken *et al.*[11].

The energy maps calculated for the various diphenyl linkages are of two types, and these have been designated as the butterfly conformation, and the twisted conformation by Anwer *et al.*[41]. These authors report very broad low energy regions centred at (±90°, ±90°) (butterfly) for sulfone and methylene linkages, and twist conformations having minimum energy with torsion angles in the range from 30 to 50° for ether and isopropylidene linkages, respectively. Our results are in excellent agreement with these, and we therefore conclude that the models are representative of real polysulfone glasses. Chain relaxation can occur by ring flips around certain linkages in the polymer backbone, but such motion is effectively hindered in ring-substituted parts.

The amorphous state order (or disorder) is presented as pair correlation functions. Analyses of the amorphous cell structures yield information on structural order, with the pair correlation function $g(r)$ giving information on the packing of the atoms in the cells, and possible long-range order. The complete characterization of amorphous polysulfones requires complete sets of pair distribution functions. For simplicity, only the total pair distribution function is considered here, although the complete analysis has been carried out. Examples of total pair correlation functions are shown in *Figure 7* for PSF and HMBIPSF. The calculations show similar results for all of the polysulfone structures considered. Maxima of $g(r)$ between 1 and 1.75 Å are typically associated with interactions between atoms in covalent bonds. These short-range-order maxima in the polysulfones are associated with the polymer backbone structure. Another important feature in the total pair correlation function of the polysulfones is the absence of sharp maxima at distances over 7 Å. The absence of peaks in this region shows that there is no correlation over, for example, biphenyl groups in the backbone, and that there is no correlation between atoms which are separated by a distance longer than 7 Å.

Cohesive energy densities were calculated, and the corresponding solubility parameters were derived from these. Values obtained for the solubility parameter, δ, are listed in *Table 1*. As could be expected they are similar for all of the modelled polysulfones. Experimental values could be found in the literature for only one of the polymers, i.e. PSF[42]. In this case, the experimental value is in excellent agreement with the calculated value, $20.0 \pm 0.5\,(\mathrm{J\,cm^{-3}})^{0.5}$. This correlation is taken as further evidence for the reliability of the constructed model.

Slight differences in the calculated solubility parameters are found between the various polymer structures in these calculations. The solubility parameter decreases as the number of methyl substituents in the polymer backbone increases. The highest values for the solubility parameters are found for PES and BIPSF, which have no methyl substituents in the polymer backbone. The interaction between the phenyl rings in the polymer backbone and between the polymer chains is strong. Relatively high values of the solubility parameters are found also for PSF and PSFP with methyl substituents only in the aliphatic isopropyl linkage between the phenyl rings. Furthermore, the difference in solubility parameters between TMPSF and TMPSFF is negligible. It is concluded that the methyl substituents in the connection between the phenyl rings affect the interaction between the rings only slightly, only increasing the stiffness of the chain. A large number of sulfone groups as connections in the polymer, e.g. in PES, increases the calculated solubility parameter compared to PSF; we therefore conclude that PES is a very rigid structure with strong interactions between the polymer chains. Replacing the isopropyl connection between the phenyl groups with an ether linkage, as in the case of PSFO, causes only a minor decrease in the solubility parameter, indicating a similar flexibility of the chains in PSF and PSFO. This is in agreement with the conclusions from the analysis of the backbone torsional angle distribution discussed above.

These considerations are further supported by the experimental values of T_g. Comparing PSF, PES and PSFO, we see that PES has a high T_g, more than 40°C higher than that of PSF and PSFO. The T_g values for PSF and PSFO differ very little. Thus, the polymer chain of PES is more rigid than that of the other two polymers, while the chain flexibility is of the same order in the latter two polymers. The T_g values for PES and BIPSF differ only by a few degrees, and they are both relatively high, as are the values of the solubility parameters for these polymers.

Comparing the values of the various solubility parameters, first for PSF and 3,4-PSF, secondly for

PSFP and PSFM, and thirdly for TMPSFP and TMPSFM, reveals that the calculated values of these parameters for the *meta*-isomers are lower than those of the *para*-isomers. The difference in chain configuration leads to different space requirements for the chains, i.e. the *meta*-configuration is kinked, and hence requires more space. This in turn leads to decreased interactions between the chains in the *meta*-isomers. The values of the T_g for the latter are also considerably lower (by 30, 50 and 40°C, respectively, in the above mentioned pairs of polysulfones) than those of the corresponding *para*-isomers, i.e. the segmental motion is greater for those isomers which require 'more space'. The occupied volumes of the *meta*- and *para*-isomers of the polysulfones has been thoroughly discussed by Aitken *et al.*[11]. Experimentally, the decreasing effect of the kinks caused by *meta*-substituted aromatic rings in the backbones of liquid crystalline polymers on their phase transition temperatures is well documented[43].

The solubility parameter decreases dramatically when the phenyl rings in the polymer backbone are substituted with methyl groups. Tetramethyl substitution causes a decrease of 1.3 $(J\,cm^{-3})^{0.5}$ for the PSF–TMPSF pair, and a decrease of 1.7 $(J\,cm^{-3})^{0.5}$ for the BIPSF–TMBIPSF pair, respectively. Hexamethyl substitution of the biphenyl moiety causes a major decrease in solubility parameter, e.g. 3.2 $(J\,cm^{-3})^{0.5}$ for the BIPSF–HMBIPSF pair. For the pairs, PSFP–TMPSFP, and PSFM–TMPSFM, the solubility parameters decrease by 1.9 and 2.4 $(J\,cm^{-3})^{0.5}$, respectively.

The free volume in the polysulfones have been probed by Voronoi tesselation statistics. Disordered systems, such as amorphous polymers, generate distributions of polyhedra of various shapes and sizes in the system. The statistical distribution of the polyhedron volumes, polyhedron surface areas, and the distribution of the shape factor (surface area/volume), constitute the description of the amorphous state. The Voronoi polyhedra are valuable depictions of the free volume distribution. The total free volume for various systems may remain the same, but variations in the free volume distribution are likely to occur.

The specific free volume, i.e. $(V - V_0)$, where V is the specific volume, and V_0 is the calculated occupied volume, and the fractional free volume (FFV), $(V - V_0)/V$, of the polysulfones have been reported in the literature[6,7,10,11,15–19]. The FFV of the polysulfones are given in *Table 1*. Methyl substituents in the aromatic rings increase the FFV values when compared to unsubstituted polysulfones. Consequently, the highest value of the FFV is found for HMBIPS. The nature of the linkage between the aromatic rings in the polysulfone diol component does not influence the FFV significantly. In polysulfones with *meta*-linked aromatic rings the FFV is in all cases lower than that of the corresponding *para*-isomer.

The distribution of the sizes of the Voronoi polyhedra in the polysulfones was further investigated. Polyhedra were constructed around every atom, including the hydrogen atoms. It was found that the distributions of the polyhedra volumes are very broad, and are bimodal or trimodal. Examples of these distribution curves are shown in *Figures 8* and *9*. The bimodal distribution of the polyhedra volumes in those polysulfones without methyl substituents in the aromatic rings is given in *Figure 8*.

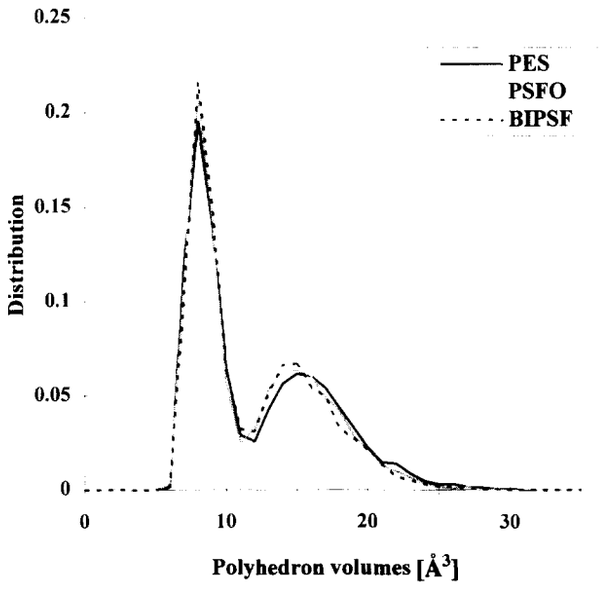

Figure 8 Distribution of the volumes of Voronoi polyhedra in PES, PSFO, and BIPSF

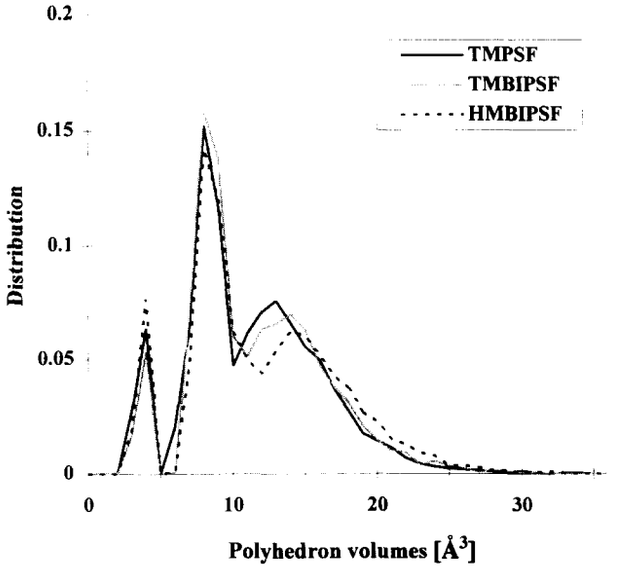

Figure 9 Distribution of the volumes of Voronoi polyhedra in TMPSF, TMBIPSF, and HMBIPSF

Major fractions of polyhedra with volumes at around 10.5 and 16 Å^3 are found in PES, PSFO and in BIPSF. No polyhedra with volumes < 7 Å^3 are found in these systems. On the other hand, the results of calculations for those polysulfones with methyl substituents in the aromatic rings, i.e. TMPSF, TMBIPSF and HMBIPSF (*Figure 9*) show a trimodal distribution of the polyhedral volumes, with a portion of very small-sized polyhedra, i.e. at around 4.5 Å^3. The amount of these small polyhedra increases as the number of aromatic methyl substituents increases in the polymer, and hence is associated with the methyl groups. The main difference, however, between the methyl substituted and the unsubstituted polysulfones, with respect to the distribution of the polyhedra volumes, is that the ring-methyl-substituted polysulfones have a larger portion of large polyhedra (> 10.5 Å^3) than those polysulfones without methyl substituents.

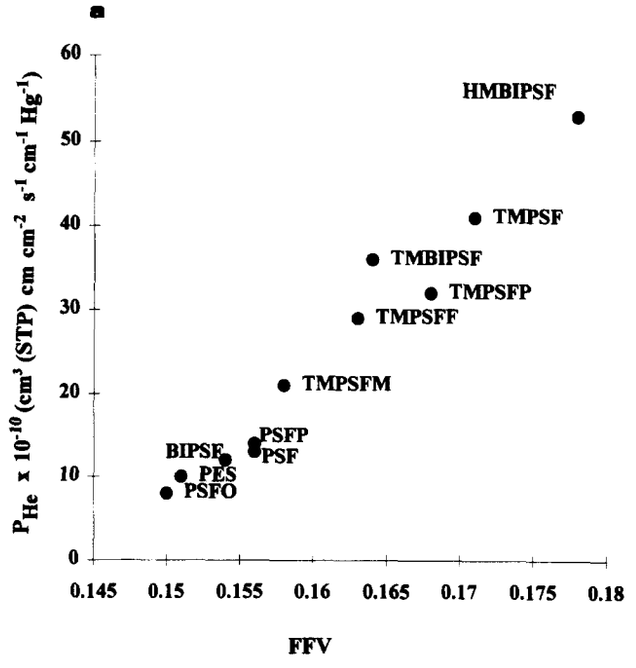

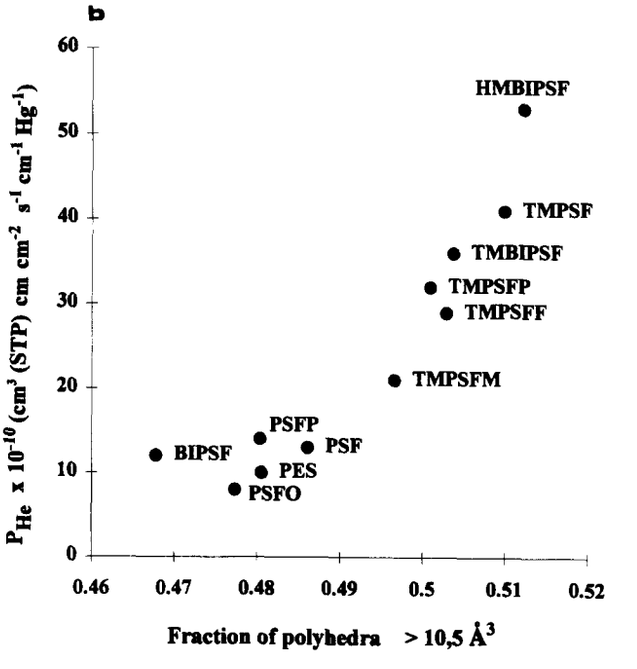

Figure 10 The permeability of helium in the various polysulfones (identified by their acronyms) as a function of: (a) free volume; (b) portion of Voronoi polyhedra > 10.5 Å^3

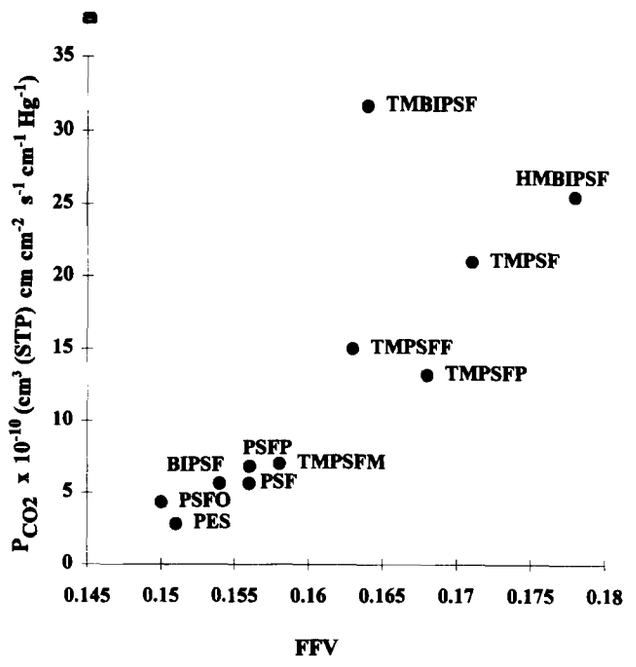

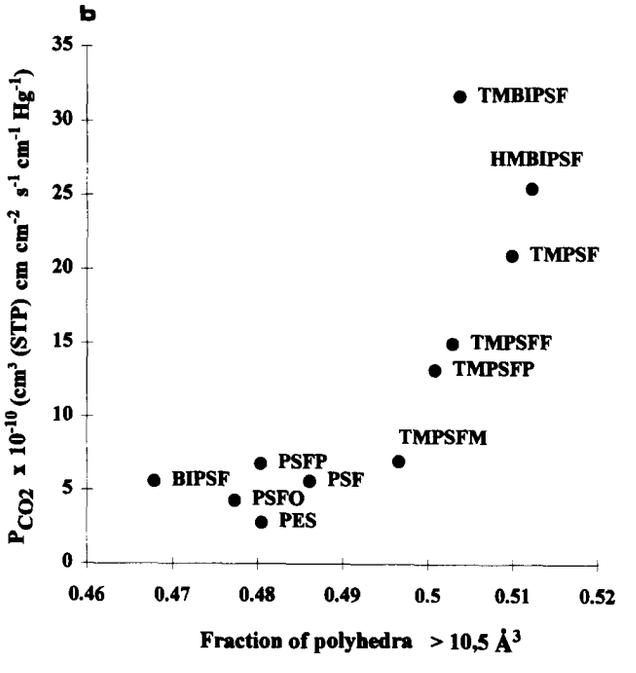

Figure 11 The permeability of carbon dioxide in the various polysulfones (identified by their acronyms) as a function of: (a) free volume; (b) portion of Voronoi polyhedra > 10.5 Å^3

Values for the FFV where the volumes are less than 10.5 Å^3 in the various polysulfones are reported in *Table 1*. These volume fractions are compared to comparable experimental values for the permeability of helium and carbon dioxide, since it can be assumed that the small-volume holes contribute less to the process of gas transport (see *Figures 10* and *11*). Clearly, the polymers form two groups, with the polymers without aromatic methyl substituents belonging to one group, and the methyl-substituted polymers belonging to another. The methyl-substituted polymers have larger portions of large-size holes, and show higher permeabilities both for helium and for carbon dioxide. The polymer TMPSFM is an intermediate case. It has a fairly large portion of large holes when compared to the other methyl-substituted polymers, but still a low permeability for both carbon dioxide and helium. The corresponding *para*-substituted polymer, TMPSFP, has a much higher permeability for these gases, although the portion of large-volume holes is of the same order of magnitude as that of TMPSFM. A similar comparison between the other two *meta*/*para*-pairs is not possible, since the gas permeability measurements have been carried out under different conditions.

The polyhedra constructed in the Voronoi tessellation method contain a centre of mass, i.e. an atom. It is therefore possible that the distribution of polyhedra is dependent on the number of different atoms in the

polymer, and therefore comparison between polymers of different chemical structure can lead to erroneous conclusions for this reason. By considering this point, values for the content (mol%) of the different atoms in the polymers were calculated. Comparison of these values with the calculated portions of the different-size polyhedra in the polymers revealed that there is no such dependence. The distribution of the volumes, therefore, is considered to be associated with the chain packing and the openess of the polymer structure.

The solubility of the different gases in the polymers influence the permeability. Since the solubility of gases and other solutes is almost constant in one class of polymers, the influence of the solubility, and the interaction between the polymer and the penetrant, can be neglected in this present kind of comparison.

The chain packing in polysulfones has been measured by using X-ray diffraction[6,7,10]. Experimental values for the *d*-spacing, a measure of the most probable intersegmental spacing, are included in *Table 1*. The validity of the constructed amorphous models in this investigation, and the conclusions drawn on the structure–gas permeability correlation, were further checked by calculating the X-ray diffraction patterns for the structures. The calculated values for the *d*-spacing are also included in *Table 1*, where it can be seen that they are in good agreement with the experimental values.

The position of the most intense peak in the X-ray diffraction pattern is taken as a measure of the most probable intersegmental spacing. The shape of the scattering peak gives further information which can be correlated to the differences in gas permeability. A broad X-ray diffraction maximum with high intensities at low angles indicates an open polymer structure, while increased intensities at higher angles is indicative of more closely packed structures. Simulated X-ray patterns from our calculations are shown in *Figures 12* and *13*. The simulated diffraction patterns show great similarity with the published experimental data[6,7,10]. *Figure 12* shows the simulated X-ray diffraction patterns for BIPSF and for HMBIPSF. BIPSF has a single absorption at a relatively high scattering angle, consistent with the low value for the FFV and the low value for the number of large holes in the structure. The scattering

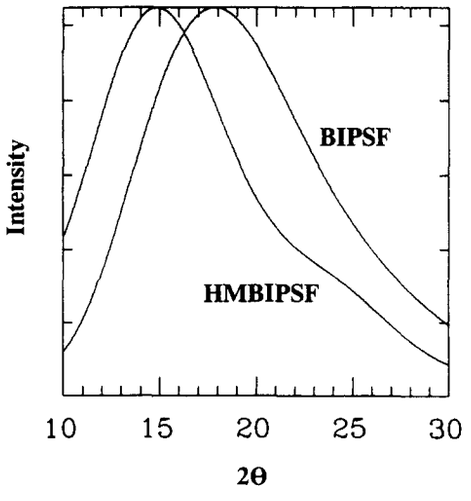

Figure 12 Calculated X-ray scattering curves for BIPSF and HMBIPSF

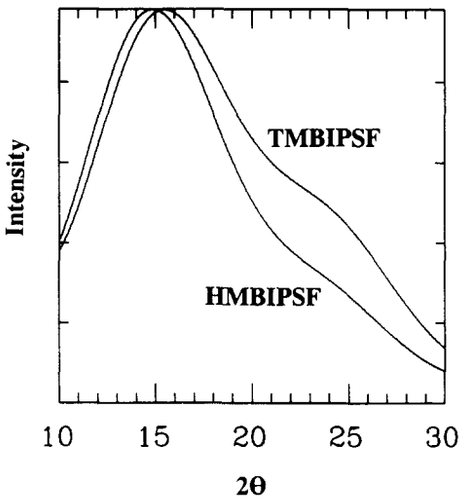

Figure 13 Calculated X-ray scattering curves for TMBIPSF and HMBIPSF

peak for HMBIPSF is much broader with its maximum at lower angles, and has a bimodal form. This is in accordance with the calculated distribution of polyhedra volumes in these polymers. Simulated X-ray patterns for TMBIPSF and HMBIPSF are compared in *Figure 13*. The values for the *d*-spacing, both experimental and calculated, show no difference between these two polymers. The FFV is, however, smaller for TMBIPSF than for HMBIPSF. This is indicated by greater intensity of the scattering at larger angles in the simulated X-ray patterns, and relates to the more closely packed structure of TMBIPSF, which contains a smaller number of large polyhedra in the structure.

CONCLUSIONS

The experimentally determined permeabilities of helium and carbon dioxide in 13 different polysulfones has been related to their chemical structure and the calculated distributions of free volume in the polymers. Molecular modelling shows that methyl substitution of the aromatic rings in polysulfones creates a wider distribution of free volume holes, leading to a more open structure with larger portions of large holes. This correlates with values for the gas permeability in the different polymers. Simulated X-ray patterns of intersegmental spacings agree well with experimental data, which further supports the conclusion regarding the role of the polymer structure on gas permeability. The molecular modelling of Voronoi polyhedra in polysulfones gives a static model of free volume distribution. This model is shown to be useful in exploring the structure–property relationship for gas permeability in polysulfones.

ACKNOWLEDGEMENT

The use of software licenses from Neste Ltd, Finland, is gratefully acknowledged.

REFERENCES

1 Koros, W. J. in 'Barrier Polymers and Structures', American Chemical Society, Washington, DC, 1990

2 Fritsche, A. K. *Polym. News* 1988, **13**, 266
3 Koros, W. J. and Chern, R. T. 'Handbook of Separation Process Technology' (Ed. R. W. Rousseau), Wiley, New York, 1987
4 Eerb, A. J. and Paul, D. R. *J. Membr. Sci.* 1981, **8**, 11
5 Ghosal, K. and Chern, R. T. *J. Membr. Sci.* 1992, **72**, 91
6 McHattie, J. S., Koros, W. J. and Paul, D. R. *Polymer* 1991, **32**, 840
7 McHattie, J. S., Koros, W. J. and Paul, D. R. *Polymer* 1991, **32**, 2618
8 Ghosal, K., Chern, R. T. and Freeman, B. D. *J. Polym. Sci. Polym. Phys. Edn* 1993, **31**, 891
9 Chiou, J. S., Maeda, Y. and Paul, D. R. *J. Appl. Polym. Sci.* 1987, **33**, 1823
10 Aitken, C. L., Koros, W. J. and Paul, D. R. *Macromolecules* 1992, **25**, 3651
11 Aitken, C. L., Koros, W. J. and Paul, D. R. *Macromolecules* 1992, **25**, 3424
12 Litt, M. H. and Tobolsky, A. V. *J. Macromol. Sci. Phys.* 1967, **3**, 433
13 Platé, N. A., Durgarjan, S. G., Khotimskii, V. S., Teplyakov, V. V. and Yampolskii, Yu. P. *J. Membr. Sci.* 1990, **52**, 289
14 Litt, M. H. *J. Rheol.* 1986, **30**, 853
15 McHattie, J. S., Koros, W. J. and Paul, D. R. *J. Polym. Sci. Polym. Phys. Edn* 1991, **29**, 731
16 Bondi, A. 'Physical Properties of Molecular Crystals, Liquids, and Glasses', Wiley, New York, 1968
17 Sugden, S. *J. Chem. Soc.* 1927, 1786
18 McHattie, J. S., Koros, W. J. and Paul, D. R. *Polymer* 1995, **33**, 1701
19 Jordan, S. S. and Koros, W. J. *Macromolecules* 1995, **28**, 2228
20 Tamai, Y., Tanaka, H. and Nakanishi, K. *Macromolecules* 1995, **28**, 2544
21 Chow, T. S. *Macromol. Theor. Simul.* 1995, **4**, 397
22 Rigby, D. and Roe, R. J. *Macromolecules* 1990, **23**, 5312
23 Theodorou, D. N. and Suter, U. W. *Macromolecules* 1985, **18**, 1467
24 Theodorou, D. N. and Suter, U. W. *Macromolecules* 1986, **19**, 139
25 Hutnik, M., Gentile, F. T., Ludovice, P. J., Suter, U. W. and Argon, A. S. *Macromolecules* 1991, **24**, 5962
26 Hutnik, M., Argon, A. S. and Suter, U. W. *Macromolecules* 1991, **24**, 5970
27 Fan, C. F. and Hsu, S. L. *Macromolecules* 1991, **24**, 6244
28 Fan, C. F. and Hsu, S. L. *Macromolecules* 1992, **25**, 266
29 Li, Y. and Mattice, W. L. *Macromolecules* 1992, **25**, 4942
30 Raaska, T., Niemelä, S. and Sundholm, F. *Macromolecules* 1994, **27**, 5751
31 Raaska, T. *PhD Thesis*, University of Helsinki, 1995
32 Allen, M. P. and Tildesley, D. J. 'Computer Simulations of Liquids', Oxford University Press, New York, 1987
33 Polymer User Guide, and Polymer Reference Guide, Version 6.0, Biosym Technologies Inc., San Diego, 1993, and Polymer User Guide Supplement, Version 7.0, 1995
34 Finney, J. L. *Proc. R. Soc. London A* 1970, **319**, 459
35 Finney, J. L. *Proc. R. Soc. London A* 1970, **319**, 479
36 Ludovice, P. J. and Suter, U. W. in 'Computational Modelling of Polymers' (Ed. J. Bicerano), Marcel Dekker, New York, 1992, p. 401
37 Brostow, W., Dussault, J. P. and Fox, B. L. *J. Comput. Phys.* 1978, **29**, 81
38 Tanemura, M., Ogawa, T. and Ogita, N. *J. Comput. Phys.* 1983, **51**, 191
39 Medvedev, N. N. *J. Comput. Phys.* 1986, **67**, 223
40 INSIGHTII and DISCOVER, molecular modelling software, Biosym Technologies Inc., San Diego, Version 2.3.0, 1993, and Version 2.3.7, 1995
41 Anwer, A., Lovell, R. and Windle, A. H. in 'Computer Simulations of Polymers' (Ed. R. J. Roe), Prentice-Hall, Englewood Cliffs, NJ, 1993, Ch. 3, p. 41
42 Brandrup, J. and Immergut, E. H. 'Handbook of Polymer Chemistry', Wiley, New York, 1974, pp. IV–353
43 Donald, A. M. and Windle, A. H. in 'Liquid Crystalline Polymers', Cambridge Solid State Science Series, Cambridge University Press, Cambridge, 1992, Ch. 3, p. 87